Capture method for digital twin of formation processes of sand bars

D. Moteki[1], T. Murai[1], T. Hoshino[2], H. Yasuda[3], S. Muramatsu[4], and K. Hayasaka[5]

[1]Graduate School of Science and Technology, Niigata University, Niigata, Japan
[2]The Civil Engineering Research Institute for Cold Region, Sapporo, Japan
[3]Research Institute for Natural Hazards & Disaster Recovery Niigata University, Niigata, Japan
[4]Electronics, Information and Communication Engineering Program, Faculty of Eng., Niigata University, Niigata, Japan
[5]Institute of Science and Technology, Niigata University, Niigata, Japan

Key Points:

- A non-contact method for measurement of the water surface and the bottom of a flume with high spatial and temporal resolution was developed.
- It is possible to provide measurement results that contribute to the clarification of the formation and development mechanism of sand waves.
- A digital twin of hydrology during formation and development of sand waves can be constructed, which is difficult with conventional methods.

Corresponding author: H. Yasuda, hiro@gs.niigata-u.ac.jp

Abstract

[The hydrological quantities governing the generation of riverbed waves (formed spontaneously on the bottoms of rivers) have been elucidated through geomorphological methods, laboratory experiments, stability analyses, numerical analyses, and other research methods. Recently, numerical analysis was performed with a fine spatial resolution. However, numerical analysis cannot always describe the real phenomena because it is based on assumptions. Therefore, understanding the physical phenomena by measurements with the same resolution as the numerical analysis is necessary. Measurement data with high resolution enable the construction of a duplicate of the measurement target on a computer, called a "digital twin". To construct a digital twin of the process of riverbed wave generation and development, the geometries of the water surface and the river bottom must be measured simultaneously. We developed and verified a measurement method for the construction of a digital twin during the generation and development of riverbed waves. The measurement system uses two cameras and a line laser to simultaneously measure the water surface and river bottom. Accurate refraction correction at the water surface is possible by acquiring the shape of the water surface, allowing the bottom shape to be determined by geometric processing. The method provides submillimeter-accurate measurements of the water surface and bottom with a spatial resolution of 0.95 cm longitudinally and 0.038 cm transversely in a 12 m $\times$ 0.45 m channel and takes only one minute per measurement. This method can provide measurement results that contribute to the understanding of the formation and development of riverbed waves.]

Plain Language Summary

[Riverbed waves, which are periodic geometric patterns that develop on the bottoms of rivers, have long been the subject of scientific research. The mechanism of their generation and development is expected to contribute to water resources engineering. However, therefore they have been analyzed by experiments and computer simulations, these waves have not been clearly explained. One of the main reasons for this is because there are few data available for hydraulic measurements in real rivers and experiments. In this study, we developed a measurement method that can obtain a larger amount of data than the ones obtained by conventional method to solve this problem. The geometries of the water surface and river bottom are obtained simultaneously using two cameras and a laser. We also confirmed that the measurement was sufficiently accurate with a high resolution in both time and space. Using the measurement data obtained by this method in combination with computer simulations, we showed that it is possible to construct a digital twin of the river surface and bed. This will make a significant contribution to the understanding of the physical mechanisms in the generation and development of riverbed waves.]

1 Introduction

Geometric shapes with strong periodicity called riverbed waves spontaneously form on river bottoms. These riverbed waves are classified into three types based on their shapes: ripples, dunes, and bars. These waves have been scientifically studied since the 19th century, using methods including geomorphological methods, model experiments, analytical methods such as stability analysis, and numerical calculations. Through these studies, results on various aspects have been obtained, including the clarification of the hydraulic quantities that govern the generation of each of the three categories of riverbed waves. In previous studies, in both model experiments and mathematical analyses, the initial bottom shape was often considered to be flat. Studies using stability analysis have highlighted that there is an innate in-

stability at the bottom of such a moving bed, which first generates riverbed waves and then spontaneously forms periodic geometries(Seminara, 2010). However, even now, it is still unclear what physical mechanism generates innate instability at the bottom of the moving bed and what physical mechanism causes the subsequent development of riverbed waves.

As mentioned above, the understanding of riverbed waves has steadily advanced using both observations in real rivers and laboratory flumes and mathematical analysis by analytical methods and numerical calculations. In particular, numerical calculations have made a significant contribution to the study of riverbed waves over the past 40 years. One of the characteristics of recent numerical calculations is that they are performed at a fine spatial resolution. The results of such analyses remind us of real phenomena. However, the governing equations in mathematical analysis, not only in numerical calculations, are derived based on certain assumptions. Therefore, there is no guarantee that the results of these analyses will describe real phenomena. Furthermore, Newton's equation of motion cannot cope with the innate uncertainty of physical phenomena (Lighthill et al., 1986). Another way to understand physical phenomena than those using physical models is based on the measurement data of the target physical phenomenon. With recent advances in measurement technology, measuring dynamic physical phenomena with a high spatial resolution is possible. Such measurement data make it possible to construct a duplicate of the measurement target on a computer, which is generally referred to as a "digital twin". For the construction of a digital twin in the process of riverbed wave generation and development, it is desirable that at least the water surface and the bottom are measured simultaneously. However, a measurement method with sufficient resolution to enable the construction of a digital twin has not yet been established, even at the laboratory scale. Note that the results obtained from detailed numerical calculations are also sometimes referred to as digital twins. However, these results are only approximate, and a true digital twin cannot be constructed. Digital twins based on measurement data are more effective for understanding and clarifying physics, where there are many unknowns.

Measurements at the experimental scale are usually performed using mechanical measurement methods, such as those using point gauges. However, considering the time evolution of moving bed hydraulics, mechanical measurement methods are not suitable because they are too slow. Therefore, recently, short-temporal measurement methods using sound waves and optical instruments have been developed. A method using sound waves has been proposed to simultaneously measure the geometry of the bottom surface and flow velocity (Thorne & Hanes, 2002; Abad & Garcia, 2009). However, this method is limited by the depth of the water, and the flow is disturbed by oscillating poles which are submerged below the water surface.

In contrast, optical methods are generally characterized as being non-contact, non-intrusive to the flow, and having high spatial resolution. So far, measurement methods have been developed for each free water surface and bottom profile in water.

The geometry of a free water surface is inherently prone to make a displacement and is easily affected by the measuring material. Therefore, it is preferred to apply optical methods that allow non-contact measurements, such as photogrammetric measurements (Chase, 1957; Benetazzo, 2006) and LiDAR (Harry et al., 2018), for sea surface and patterned light projection (Lipeme Kouyi et al., 2003; Watanabe et al., 2011) and monochromatic lasers (Legout et al., 2012) for laboratory flumes. Photogrammetry and patterned light projection can be used to measure the geometry of an object surface in a short time and with high accuracy, but only the water's surface can be measured; it is difficult to measure the bottom surface at the same time as the water surface.

The measurement of the bottom geometry by optical methods can be broadly classified into methods using photogrammetry (Lane et al., 2001; Butler et al., 2002) and those using monochromatic lasers (González et al., 2007; Yeh et al., 2009; Di Risio et al., 2010; Huang et al., 2010; Visconti et al., 2012; de Ruijsscher et al., 2018). For the measurement of bottom geometries using lasers in laboratory flumes, drybeds (Yeh et al., 2009), still water (Di Risio et al., 2010), and flowing water (Visconti et al., 2012) use point lasers. As an extension of the above, dry beds and still water (González et al., 2007) and flowing water (de Ruijsscher et al., 2018) have been measured using a line laser. González et al. (2007) showed that the geometry of the bottom surface in still water can be accurately measured based on triangulation using a combination of line laser and CCD camera, with refraction correction according to Snell's law. de Ruijsscher et al. (2018) measured the bottom surface in flowing water using a line laser and a 3D camera and mentioned that refraction correction can be used to accurately measure the bottom surface in moving bed flows in which the water is not deep. In a laboratory experiment, Legout et al. (2012) showed that by adding titanium dioxide to water and increasing the laser reflection intensity at the water surface, the geometry of the water surface can be measured with high accuracy using a line laser and CCD based on triangulation. Huang et al. (2010) showed that water depth and the bottom surface can be measured simultaneously with submillimeter accuracy using a line laser to measure the bottom geometry and the fluorescence brightness of colored water to measure the water depth. Their method also showed excellent time resolution. However, because the relationship between the fluorescence brightness of the colored water and the water depth is exponential, it was not possible to avoid changes in accuracy depending on the water depth, and the range of application was limited to the measurement of very shallow streams with a water depth of a few millimeters. It is difficult to measure the process of the generation and development of riverbed waves using their method because the flows that form riverbed waves are often several centimeters deep in the laboratory.

As mentioned above, the measurement principle based on triangulation using a laser and a camera can be employed to measure the water surface and the bottom of the moving bed hydrograph with high accuracy; however, no study has acquired both at the same time to the best of our knowledge. In this study, we developed and verified a measurement method to construct a digital twin under hydraulic conditions in which riverbed waves are formed. The measurement device is called stream tomography (ST) based on its principle. ST takes a non-contact method for monitoring the geometries of the water surface and bottom with high spatial and temporal resolution in the same three-dimensional space. We also quantified the formation process of riverbed waves in moving bed experiments, showing that the measurement may be able to explain the generation mechanism of riverbed waves. Section 2 describes the measurement principle and the setup of the experimental facilities. Section 3 presents the measurement results and evaluates the accuracy and applicability. Section 4 discusses the application to moving-bed experiments and validation of the numerical model. Finally, Section 5 provides a summary of the paper. In this study, only swept sand is considered, not suspended sand.

2 Measurement principles

2.1 measurement requirements

To obtain a pair of bathymetric and bottom geometries, it is sufficient to measure the water surface and underwater bottom geometries simultaneously as corresponding data. Such a hydraulic measurement should satisfy the following four requirements. First, it must be noncontact so as not to affect the hydraulic phenomena. Second, the temporal resolution must be sufficiently high to allow us to consider that the bottom is a pseudo-fixed bed during a single measurement (i.e., suffi-

ciently faster than the advection velocity of the bottom (Callander, 1969; Seminara, 2010): approximately 1 min or less under the hydrographic conditions described below). Third, to maintain the simultaneity of measurements, the measured hydraulic quantities should correspond in time and space. Fourth, the spatial resolution should be as high as or higher than that of the hydraulic calculation (less than the calculation grid size (1 cm $\times$ 1 cm) used in general numerical analysis (the finer the better)), under the assumption of the calculation using a model of other hydraulic quantities such as flow rate.

2.2 Equipment configuration

2.2.1 Optical configuration for the measurement

To acquire the geometric data of the water surface and the bottom simultaneously, the ST was configured to use a laser sheet and two cameras. The laser is a YAG laser with a wavelength of 532 mm. The oscillated laser beam was formed into a sheet using a lens and irradiated vertically across the channel. For the cameras, two Raspberry Pi camera modules v2 were used. To enable remote control of the cameras, video recording in this measurement method was performed at a frame rate of 40 fps and a resolution of 720p, based on the performance limitations of the Raspberry Pi. To prevent unintentional diffuse reflection of illumination on the water surface, the laboratory operated as a dark room during the measurement.

2.2.2 moving carriage with electric control

The aforementioned optical instruments, except the laser oscillator, were fixed to a carriage moving on a track set parallel to the channel, as shown in Figs. 1,2. The laser sheet was irradiated vertically from 100 cm above the channel. The cameras were placed facing each other across the irradiated laser sheet. The camera was set at an angle of 56° downward to the flume. The moving speed of the traveling platform was adjustable with a maximum speed of 2.5 m/sec.

2.2.3 Equipment control

For measurement, the camera and carriage must be controlled simultaneously. In general, laboratory experiment on moving bed hydraulics take a long time, and while controlling the measurement time interval accurately is important, the operation is complicated. Raspberry Pi was incorporated in the control unit of this measurement system, and the carriage and camera were controlled from a local server. This allows unattended measurements to be taken at precise time intervals. Because the camera module of Raspberry Pi takes several seconds to start up, the carriage was operated with a delay of several seconds. To synchronize the timing of the two cameras, the laser was blocked by a board at the starting point of the measurement, and the cameras detected the laser irradiated on the bottom of the channel after the carriage started moving. In this way, the timing of the two cameras was synchronized within 1/80 s.

2.2.4 Spatial and temporal resolution

The spatial resolution of this measurement method is different for the specified conditions in the transverse and longitudinal directions. The spatial resolution in the transverse direction was specified by the number of pixels in the captured image, which depends on the resolution of the optical sensor mounted on the camera and is 0.039 cm. The spatial resolution in the longitudinal direction is defined by the combination of the moving speed of the carriage and the frame rate of the cameras, and the resolution gets higher as either of these increases. The temporal resolution

is correlated with a combination of the shooting range in the longitudinal direction and the speed of the carriage. Therefore, the moving speed of the carriage must be sufficiently faster than the advection velocity of the bottom surface to maintain spatial continuity during the measurement, whereas the resolution in the longitudinal direction is less than the grid size commonly used in hydraulic analysis. Under the conditions for which this system is designed, the water depth often observed in experiments is approximately 3 cm, and the approximate bottom advection velocity is 5.0×10^{-4} m/sec (Seminara, 2010). In this study, the carriage speed was set to 0.38 m/sec, considering the aforementioned constraints. The speed of the carriage can measure a 10 m flume in 27 s, and the spatial resolution in the longitudinal direction is 0.95 cm. The minimum temporal resolution is approximately 1 min because the system measures only the outward direction.

2.3 Physical principles

This measurement method is based on the principle of triangulation, in which three-dimensional coordinates are obtained from the intersection of two geometric vectors connecting two known points and a measurement target. In this study, the vectors of the directed line segments are referred to as geometric vectors. The geometric relationship in this method is shown in Fig. 3. The water surface level can be calculated as the intersection h of two geometric vectors connecting the origin coordinates of each of the two cameras and the laser reflection coordinates of the water surface, and the water bottom level is calculated as the intersection b of two geometric vectors connecting the water surface level and the laser reflection coordinates of the water bottom level. Of these, the calculation of the 3-D coordinates of the water bottom level requires consideration of refraction at the water surface. In this method, the refraction of the reflected laser beam at the bottom of the water surface is corrected based on Snell's law, and the 3-D coordinates of the bottom level are obtained based on the water surface level that can be obtained areally. The measurement procedure comprises the following four steps: 1) video recording with two cameras while the carriage is moving in the downstream direction, 2) analysis of the intersection points between the laser sheet and the water/bed surface in the videos, 3) calculation of the water surface level h based on triangulation, and 4) calculation of the bed level b by correction based on Snell's law. The internal and external parameters of the camera required as the origin of the calculation were calculated using Zhang's calibration method(Zhang, 2000). The origin coordinates of the two cameras were calculated for upstream C_u and downstream C_d, respectively. C_u and C_d are number vectors with 3-D spatial coordinates as components, $C_u = (x_{c_u}, y_{c_u}, z_{c_u})$ and $C_d = (x_{c_d}, y_{c_d}, z_{c_d})$.

2.4 Image analysis

To measure the geometries of the water surface and the water bottom, pixel numbers corresponding to the water surface and bed surface were detected in the captured images. The taken images are shown in the upper part of Fig. 4, and the examples of water surface and bottom detection are shown in the lower part. In the figure, i and j represent the pixel numbers in the horizontal and vertical directions of the image, respectively. The pixel number corresponding to the intersection of the laser sheet and the water surface was detected using Canny, a function of OpenCV(https://opencv.org), and by specifying the green lightness range as the threshold. Similarly, the pixel number corresponding to the intersection of the laser sheet and the bed surface was detected as the maximum value of the green lightness in the j-direction. The reflectance intensity of the green luminosity at the water surface and bottom varies depending on the experimental environment, the intensity of the laser beam, and the riverbed material. In particular, the detection threshold of

the water surface must be adjusted according to the measurement conditions. In this study, the water surface detection threshold was set to a range in which the green luminosity exceeded 40 but did not exceed 160.

2.5 Obtaining the water surface gradient for refraction correction

This subsection presents a procedure for calculating the water surface gradient required for the calculation of the bed level by refraction correction based on Snell's law, using a grid of water surface measurements. Numerous water surface measurements can be conducted in the longitudinal and transverse directions with the spatial resolution described above. Because a gradient of the water surface is required for refraction correction of the bed surface measurement, a structured discrete function $H_{(i,j)}$ is created by arranging h in Fig. 3 in a grid of arbitrary intervals (Fig. 5). The bed level b was calculated from the geometric relationship shown in Fig. 6. Accurate refraction correction requires C_{hu} and C_{hd}, as shown in Fig. 6, and the water surface slope (normal vector of the water surface) n_u and n_d at that point. $C_{hu}(C_{hd})$ is the intersection vector between, the vector connecting $C_u(C_d)$ and the identified pixel at the bottom, and the water surface. Because $n_u(n_d)$ represents the water surface gradient at $C_{hu}(C_{hd})$, it can be calculated using $H_{(i,j)}$. The refractive indices used for refraction correction were air ($n_{air} = 1.0$) and water ($n_{water} = 1.333$), respectively.

3 Validation

The following experiments were conducted to verify the accuracy and applicability of ST. Experiments 1 to 3 were conducted without sand using objects of known shapes (Fig. 7), and Experiment 4 was conducted in a flow over a sand wave of the scale often observed in experiments on sandbars. To verify the accuracy of measurement, the plane of the rectangular top surface placed on the bottom, as shown in Fig. 7, was used because the true shape of the flume bottom was unknown. The measurement principle of ST is such that the measurement error becomes large when the geometric shape of the bottom surface abruptly changes in the longitudinal direction, and a blind spot exists in the view of the camera. Therefore, hemispheres were used for verification to confirm the follow-up of the measurements in the longitudinal direction. The hemisphere has an infinite divergence with the bed slope at the point of contact with the bottom. The size of the hemisphere is $r = 2.5$ cm, which is larger than the maximum wave height of the sand waves (=2 cm), as confirmed in the preliminary experiments. The flow depth in experiments 1 to 3 was set to be 1.5 cm to 4 cm in the measurement range as a condition for the hemisphere to be underwater. The flow depth in the experiments on sand bars in this flume was approximately 1 cm to 3 cm. In Experiment 4, the bottom of the channel was covered with 5 cm of silica sand ($D_{50} = 0.755$ mm), which is commonly used in moving-bed experiments, and the discharge was 2.5 L/sec for 2 hours to confirm the formation of sandbars. After that, the sandbar was drained and fixed with cement.

3.1 Experiment 1 (dry)

The purpose of Experiment 1 was to verify the validity of the triangulation-based ST and its angular tracking capability.

In the upper part of Fig. 8, the plane of the rectangle was measured five times, and the measurement results are shown in three measurement lines for the longitudinal and transverse directions. The lines were set at 3 cm intervals for both longitudinal and transverse measurements. The upper solid line in Fig. 8 is an estimate obtained from the least-squares method of the measurement results and is regarded

as the true value in the evaluation of this section. The true value lines are skewed in both longitudinal and transverse sections, but this is due to the skewness of the measuring device or the water channel and is unrelated to the measurement accuracy. The measurement error of the triangulation is shown by the difference from the true value in the lower part of Fig. 8. The error of the measurement was less than 0.03 cm at all measurement points in each longitudinal and transverse direction.

To verify the angular-tracking properties, Fig. 9 shows the measurement results of three hemispheres lined up in the longitudinal direction and the solid line of the true value superimposed. The measurement results are shown by superimposing the results of five measurements in three hemispheres (15 measurements in total). The vertical error of each measurement is shown on the right side of Fig. 9. While the error was less than 0.1 cm near the hemisphere apex, the accuracy deteriorated as the angle to the bottom increased or decreased. Using an error of 0.2 cm as a threshold, the following angle was calculated to be approximately 60°, which is consistent with the camera's overhead angle. The accuracy is lower for hemispheres than for rectangles because the timing of the camera shots cannot be perfectly matched.

3.2 Experiment 2 (Still water)

Experiment 2 was conducted to verify the validity of the ST water surface measurements and bottom measurements with refraction correction.

In the upper part of Figs. 10,11, the measurement results of the hydrostatic surfaces of three measurement lines in the longitudinal and transverse directions and the estimated values obtained by the least-squares method as true values as in 3.1 are shown as solid lines. The position of the measurement line in the transverse direction was $x = 100, 200, 300$ cm with $x = 0$ cm as the starting point. The position of the measurement line in the longitudinal direction was $y = 7.5, 22.5, 37.5$ cm with $y = 0$ cm on the right bank of the channel. The error from the true value is shown in the lower part of Figs. 10,11. The measurement results include a characteristic error which seems to be affected by the movement of the carriage, but the cause remains unknown. Figs. 12,13 show the histograms of the errors in the longitudinal and transverse directions of the water surface, respectively, with the sum of the three lateral segments. The magnitude of the error varies depending on the location, but it is less than 0.05 cm for most of the longitudinal transects and about 0.1 cm at the maximum.

Fig. 14 shows the measurement results of the hemisphere in still water and the solid line of the true value, as in Subsection 3.1, overlaid with results of 15 measurements. The measurement of the bottom surface in still water requires refraction correction based on the measured values at the water surface, but there was no degradation in accuracy. In addition, the angular follow-up was approximately the same.

3.3 Experiment 3 (Flowing water)

Experiment 3 was conducted to verify the validity of the measurements under flowing water conditions. Fig. 15 shows the measurement results of the hemisphere at the bottom of the flowing water condition and the solid line of the true value, superimposed with the results of 15 measurements as in Subsection 3.1. The measurement accuracy and angular follow-up remained almost unchanged from those in the dry and still water conditions.

3.4 Experiment 4 (Flowing water with fixed sandbed)

Experiment 4 was conducted to validate the geometry measurements on a sandy riverbed. The bottom of the river was cemented after being drained with water, as described above. The results shown in Fig. 16 are the measurement results at the bottom dry section and are regarded as the true values in this section. The contours in Fig. 17 show the measured geometries of the water surface and the bottom under the condition of water flow on the fixed bottom surface. The contour area was trimmed by 1 cm on each side near the wall in the transverse direction. In the water surface measurement results, we assumed that the influence of the movement of the carriage, which was confirmed by Subsection 3.2, exists, but it could not be confirmed because of the larger disturbance of the water surface caused by water flow. In the measurement of the bottom surface, as shown in Fig. 17, noise was observed in the entire area. This noise was caused by water flowing under the thin layer of cement used to fix the geometric shape of the bottom surface, causing the entire surface to float. Measurements such as $x = 300$ cm,$y = -15$ cm coincide with the area where the cement was detached by the flow, as observed during the experiment. There are some missing points near the left and right walls, which may have been caused by the wall. At $y = -20$ cm, the bottom shape was measured to be higher than that of the dry shape. Fig. 18 shows the contour of the difference from the bottom surface measured with dry as the true value. The areas where the measurement accuracy decreased were concentrated at the points where the bottom slope changed abruptly, and the errors that exceeded the trackable angle could be observed on the left bank at 380 cm. Most of the errors were less than 1 mm.

4 Discussion

As described above, ST can measure the geometries of the water surface and bottom with high accuracy even in flowing water, although the accuracy decreases in places where the bottom slope changes abruptly from the formation of alternating sandbars. Hereafter, the geometries of the water surface and bottom during the development of the alternating bar were quantified by measuring them in experiments under the formation conditions of the alternating bar. The implications of the hydraulic data obtained by ST are also discussed.

The geometries of the water surface and bottom under alternating sandbar formation conditions were measured with high temporal resolution using ST. The measurements were taken at 1-min intervals but are presented at arbitrary intervals to save paper space. In the experiment, the channel slope was set at 1/160 and the flow rate from the upstream end was 2.0 L/sec. The river bed was covered with 5 cm thick silica sand ($D_{50} = 0.755$ mm), and no sand was supplied. Fig. 19 shows the measurement results within the range without the influence of the upstream and downstream edges. The figure is trimmed by 2.5 cm because the measurement near the wall is unstable. The positional relationship between the water surface and bottom of Fig. 19 is independent of water depth.

There was no significant difference from the measurements in the previous verification of the fixed bed, and the measurement results can be deemed valid. The water surface and bottom levels are shown by the blue and brown surfaces in Fig. 19, respectively. As time progresses, the development of periodic alternating sand bars from the initial flat bed can be seen in the measurements.

Five minutes after the start of the experiment, periodic undulations with wavelengths much smaller than those of the alternating sand bar were formed across the entire water surface and bottom. This depth-scale undulation was observed at all times, especially at 40 min when the wave height reached approximately 1 cm on the

right side at 300 cm. In addition, at 40 min, the formation of a clear sandbar at the bottom near 300 cm was observed. This sandbar then drifted downward and grew in height with time, and a corresponding undulation of the water surface was observed.

Hydraulic analysis using the shallow water equation and the bed load function is usually performed to understand the hydrology of sandbars. However, neither of these methods has been sufficiently verified and validated (V&V) because there is no method to measure hydraulic phenomena with the same temporal and spatial resolution as that of hydraulic analysis. In particular, various forms of the bed-load function have been proposed (e.g., Meyer-Peter & Müller (1948); Ashida & Michiue (1972)), but all of them are discussed on the logarithmic axis, and their validity is questionable. To perform V&V of the above model in a laboratory channel, the water depth or flow velocity must be measured in addition to the bottom profile. The measurement of flow velocity is very difficult because it is a vector quantity that has a three-dimensional spatial distribution on the riverbed waves. ST can measure the water depth and bottom shape with the same spatial and temporal resolution as the hydraulic analysis and can be verified and validated.

ST measurements of moving bed hydrodynamics can quantify phenomena with a spatial and temporal resolution which is difficult to achieve using conventional measurement methods such as point gauges and sonic devices. Such data enables the first application of data-driven time series analysis to the hydrodynamics of riverbed waves, and shows the possibility of understanding the mechanism of riverbed wave generation. In addition, if higher resolution measurements are required in the future, higher frame rate cameras or multiple cameras can easily be used to achieve this. Two-dimensional estimation of flow velocity is possible by combining the measured data with numerical analysis, which enables highly accurate replication of model experiments in cyberspace. It is possible to construct a digital twin of the hydrodynamics during the formation and development of riverbed waves, which has been difficult using conventional methods.

5 Conclusion

In this study, we developed a non-contact, simultaneous measurement method with high spatial and temporal resolution for geometries of the water surface and bottom during the generation and development of riverbed waves at the bottom of a laboratory flume. The developed method was demonstrated to have sufficient measurement accuracy. However, the measurement accuracy decreases at places where the bottom slope changes abruptly, which poses a problem. This method can provide measurement results that contribute to the elucidation of the formation and development mechanism of riverbed waves and can be used to construct a digital twin for this physical process.

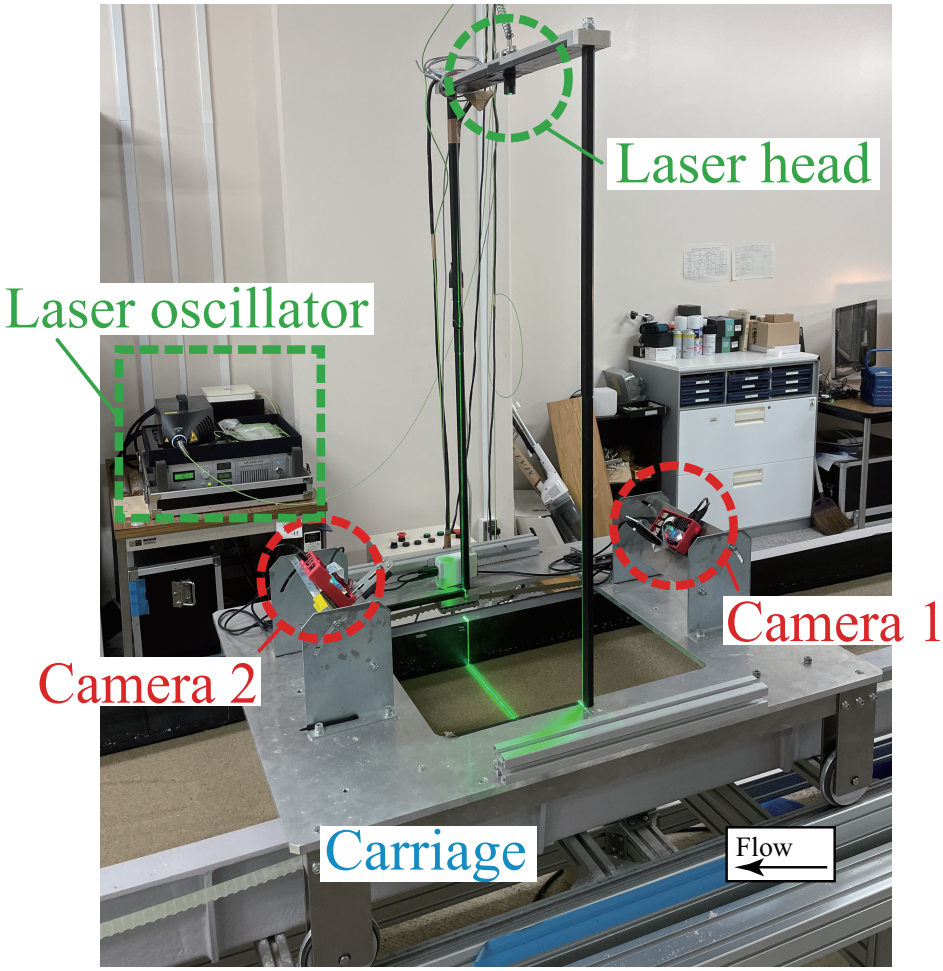

Figure 1. Equipment layout of the measuring device.

Acknowledgments

The raw data used for Section 3 to 4 in this study are available at 4TU.ResearchData via https://doi.org/10.4121/16758646 with CC BY-NC (Attribution-NonCommercial). This work was supported by JSPS KAKENHI Grant Numbers JP21H04596, JP20K20543, and JICE(No.19005 and No. 20004), Japan Institute of Country-ology and Engineering. For details of the data, please refer to the enclosed README.md. We would like to thank Editage (www.editage.com) for English language editing.

References

Abad, J. D., & Garcia, M. H. (2009). Experiments in a high-amplitude kinoshita meandering channel: 1. implications of bend orientation on mean and turbulent flow structure. *Water Resources Research*, *45*(2). doi: 10.1029/2008WR007016

Ashida, K., & Michiue, M. (1972). Study on hydraulic resistance and bed-load transport rate in alluvial streams. *Proceedings of the Japan Society of Civil Engineers*, *1972*(206), 59-69. doi: 10.2208/jscej1969.1972.206_59

Benetazzo, A. (2006). Measurements of short water waves using stereo matched image sequences. *Coastal Engineering*, *53*(12), 1013-1032. doi: 10.1016/j.coastaleng.2006.06.012

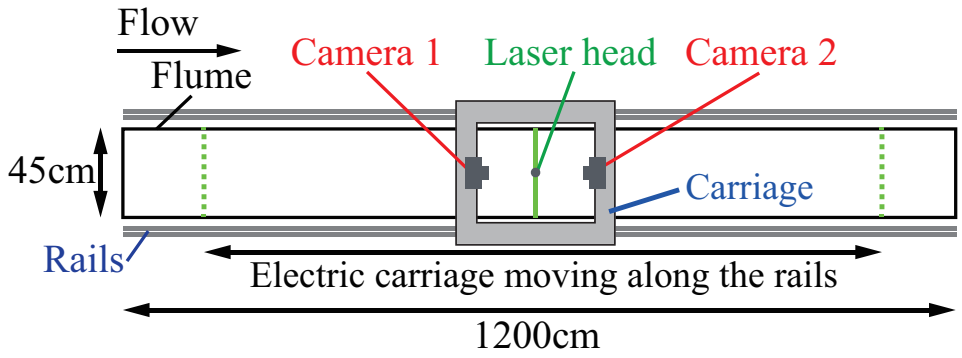

Figure 2. Plan view of the measuring device and flume.

Butler, J., Lane, S., Chandler, J., & Porfiri, E. (2002, APR). Through-water close range digital photogrammetry in flume and field environments. *PHOTOGRAMMETRIC RECORD*, *17*(99), 419-439. doi: 10.1111/0031-868X.00196

Callander, R. A. (1969). Instability and river channels. *Journal of Fluid Mechanics*, *36*(3), 465–480. doi: 10.1017/S0022112069001765

Chase, L. M. W. M. E. P. W. R. F. S. G. V. R. W. R., J. Cote. (1957). *The directional spectrum of a wind generated sea as determined from data obtained by the stereo wave observation project* (Tech. Rep.). Retrieved from `https://www.biodiversitylibrary.org/item/86687` (https://www.biodiversitylibrary.org/bibliography/39092)

de Ruijsscher, T. V., Hoitink, A. J. F., Dinnissen, S., Vermeulen, B., & Hazenberg, P. (2018). Application of a line laser scanner for bed form tracking in a laboratory flume. *Water Resources Research*, *54*(3), 2078-2094. doi: 10.1002/2017WR021646

Di Risio, M., Lisi, I., Beltrami, G., & De Girolamo, P. (2010). Physical modeling of the cross-shore short-term evolution of protected and unprotected beach nourishments. *Ocean Engineering*, *37*(8–9), 777–789. doi: 10.1016/j.oceaneng.2010.02.008

González, E. P., Díaz-Pache, F. S.-T., Mosquera, L. P., & Agudo, J. P. (2007). Bidimensional measurement of an underwater sediment surface using a 3d-scanner. *Optics & Laser Technology*, *39*(3), 481-489. doi: 10.1016/j.optlastec.2005.11.007

Harry, M., Zhang, H., Lemckert, C., Colleter, G., & Blenkinsopp, C. (2018). Observation of surf zone wave transformation using lidar. *Applied Ocean Research*, *78*, 88-98. Retrieved from `https://www.sciencedirect.com/science/article/pii/S0141118718300671` doi: 10.1016/j.apor.2018.05.015

Huang, M. Y. F., Huang, A. Y. L., & Capart, H. (2010). Joint mapping of bed elevation and flow depth in microscale morphodynamics experiments. *Experiments in Fluids*, *49*(5), 1121–1134. doi: 10.1007/s00348-010-0858-4

Lane, S. N., Chandler, J. H., & Porfiri, K. (2001). Monitoring river channel and flume surfaces with digital photogrammetry. *Journal of Hydraulic Engineering*, *127*(10), 871–877. doi: 10.1061/(ASCE)0733-9429(2001)127:10(871)

Legout, C., Darboux, F., Nédélec, Y., Hauet, A., Esteves, M., Renaux, B., ... Cordier, S. (2012). High spatial resolution mapping of surface velocities and depths for shallow overland flow. *Earth Surface Processes and Landforms*, *37*(9), 984-993. doi: 10.1002/esp.3220

Lighthill, M. J., Thompson, J. M. T., Sen, A. K., Last, A. G. M., Tritton, D. J., Mason, B. J., ... Westcott, J. H. N. (1986). The recently recognized failure of predictability in newtonian dynamics. *Proceedings of the Royal Soci-*

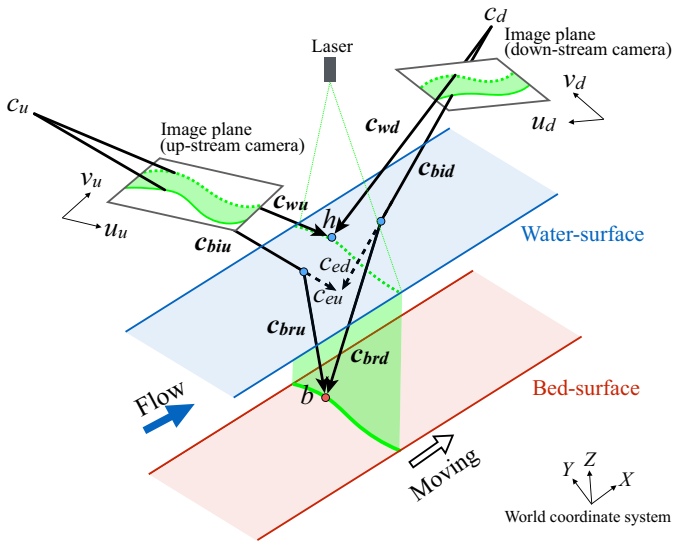

Figure 3. Outline of geometric relations. C_u and C_d are the camera positions. h is calculated by observing the laser reflection on the water surface and is the intersection of the two observation vectors C_{wu} and C_{wd}. Reflection on the bed surface is observed at the position where it is refracted by the camera, $C_{biu} + C_{eu}(C_{bid} + C_{ed})$. By correcting the refracted reflection vector of the bed surface at the intersection point with the water surface, the observed vector of the bed surface becomes $C_{biu} + C_{bru}(C_{bid} + C_{brd})$.

ety of London. A. Mathematical and Physical Sciences, *407*(1832), 35-50. doi: 10.1098/rspa.1986.0082

Lipeme Kouyi, G., Vazquez, J., & Poulet, J.-B. (2003, 06). 3d free surface measurement and numerical modelling of flows in storm overflows. *Flow Measurement and Instrumentation*, *14*, 79-87. doi: 10.1016/S0955-5986(03)00011-6

Meyer-Peter, E., & Müller, R. (1948). Formulas for bed-load transport. *2nd Meeting of International Association for Hydraulic Research, Stockholm*, 39–64.

Seminara, G. (2010). Fluvial sedimentary patterns. *Annual Review of Fluid Mechanics*, *42*(1), 43–66. doi: 10.1146/annurev-fluid-121108-145612

Thorne, P., & Hanes, D. (2002, MAR). A review of acoustic measurement of small-scale sediment processes. *CONTINENTAL SHELF RESEARCH*, *22*(4), 603-632. doi: 10.1016/S0278-4343(01)00101-7

Visconti, F., Stefanon, L., Camporeale, C., Susin, F., Ridolfi, L., & Lanzoni, S. (2012). Bed evolution measurement with flowing water in morphodynamics experiments. *Earth Surface Processes and Landforms*, *37*(8), 818-827. doi: 10.1002/esp.3200

Watanabe, Y., Mitobe, Y., & Oshima, K. (2011, 12). An imaging technique for measuring wave surface shapes. *Coastal Engineering Journal*, *53*. doi: 10.1142/S0578563411002458

Yeh, P.-H., Chang, K.-A., Henriksen, J., Edge, B., Chang, P., Silver, A., & Vargas, A. (2009). Large-scale laboratory experiment on erosion of sand beds

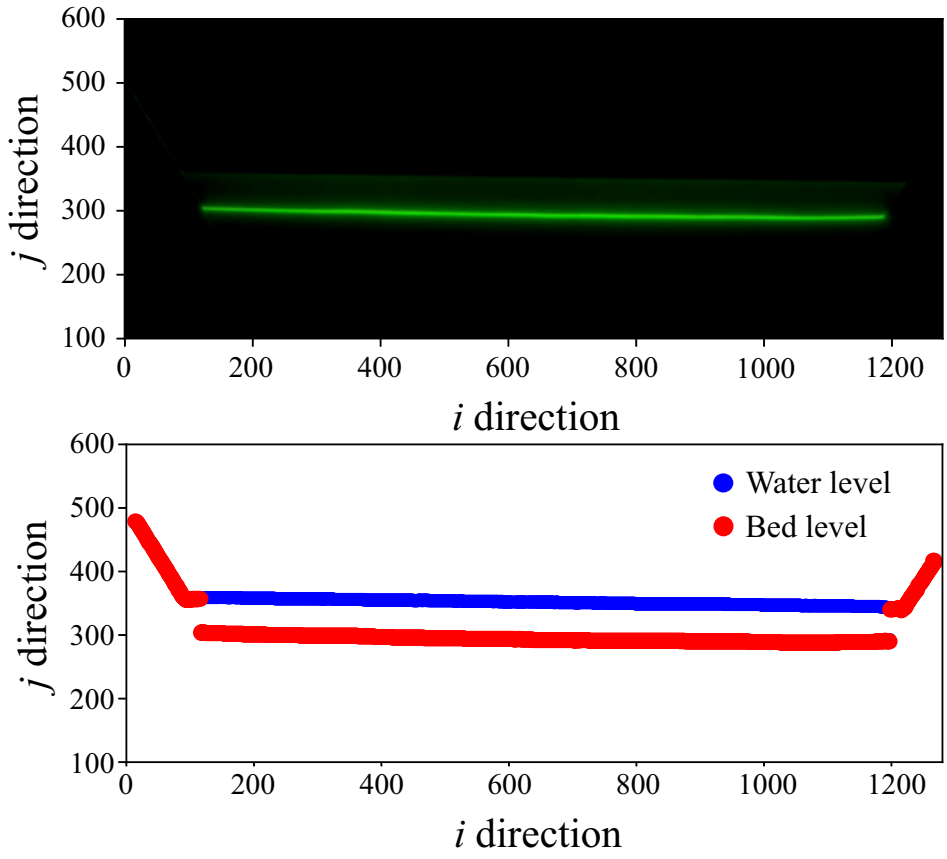

Figure 4. (Upper) Raw imaged taken from the downstream camera. (Lower) Water surface and bed detection positions using green lightness as a threshold. In this figure, i and j are the pixel numbers of the image in the horizontal and vertical directions, respectively.

by moving circular vertical jets. *Ocean Engineering*, *36*(3–4), 248–255. doi: 10.1016/j.oceaneng.2008.11.006

Zhang, Z. (2000). A flexible new technique for camera calibration. *IEEE Transactions on Pattern Analysis and Machine Intelligence*, *22*(11), 1330-1334. doi: 10.1109/34.888718

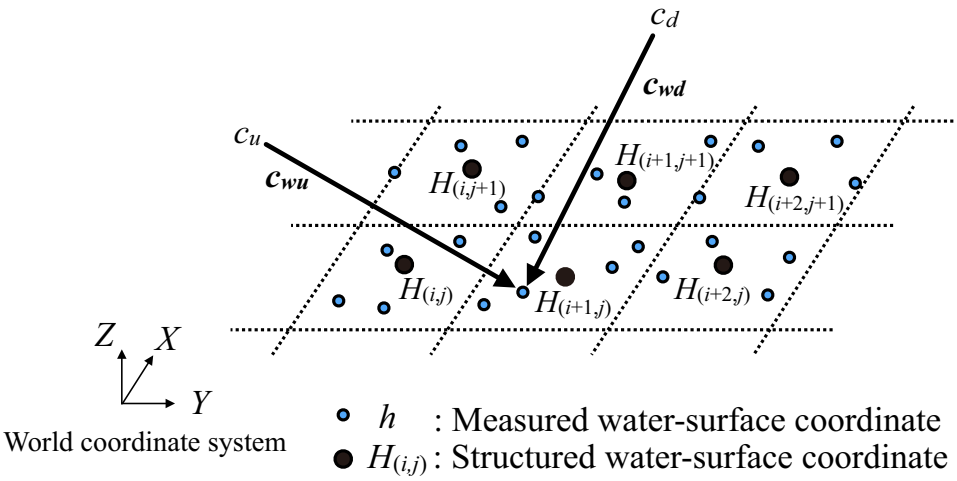

Figure 5. The structure-type function of the water level $H_{(i,j)}$, which is used for the refraction correction, is created from the calculated point cloud of h using the nearest point of the structure grid center coordinates.

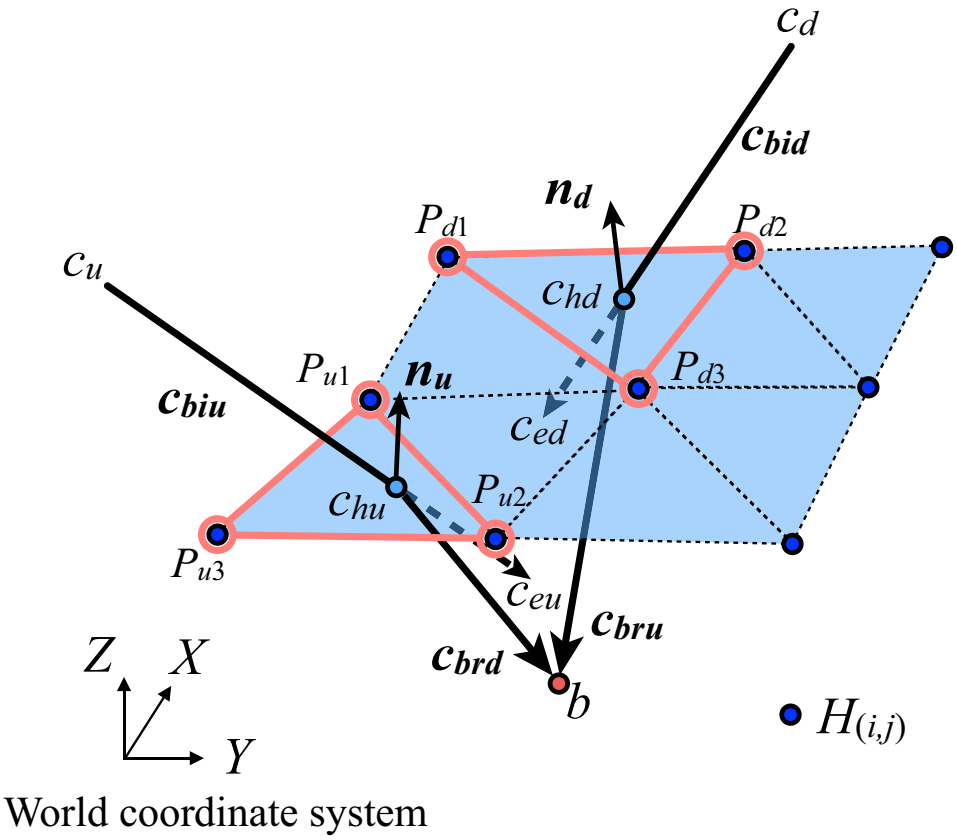

Figure 6. Schematic representation of the geometric relations in refraction correction. The refraction correction based on Snell's law requires the water surface gradient $n_u(n_d)$ at $C_{hu}(C_{hd})$. The water levels P_{u1}, P_{u2}, an P_{u3} (P_{d1}, P_{d2}, and P_{d3}) at the three surrounding points are used to calculate $n_u(n_d)$.

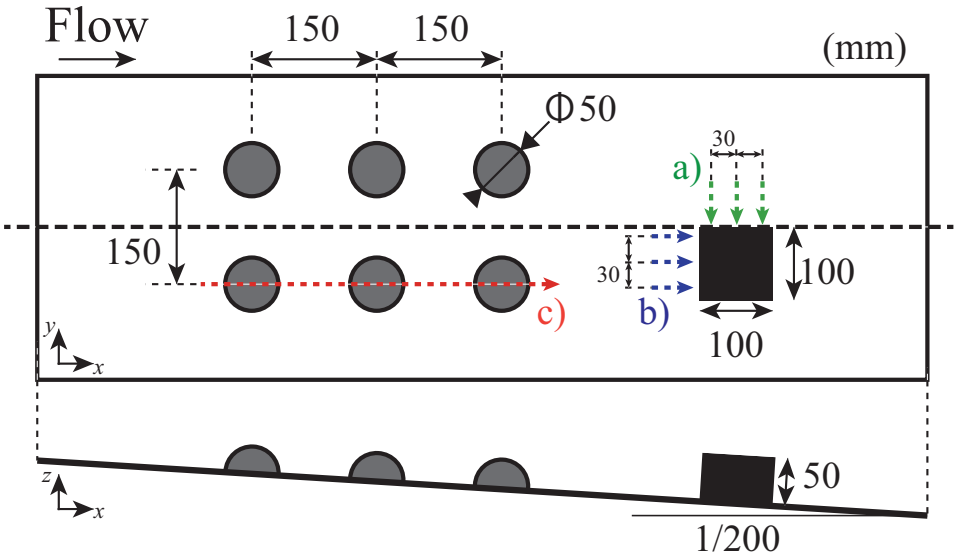

Figure 7. Arrangement of the objects for fixed-floor verification. The upper and lower panels show the overhead and cross-sectional views of the channel, respectively. The radius of the hemisphere is 25 mm, and the dimensions of the rectangle are 100×100×50 mm(width×length×height). The arrows a), b), and c) indicate the measurement lines in the subsequent verification.

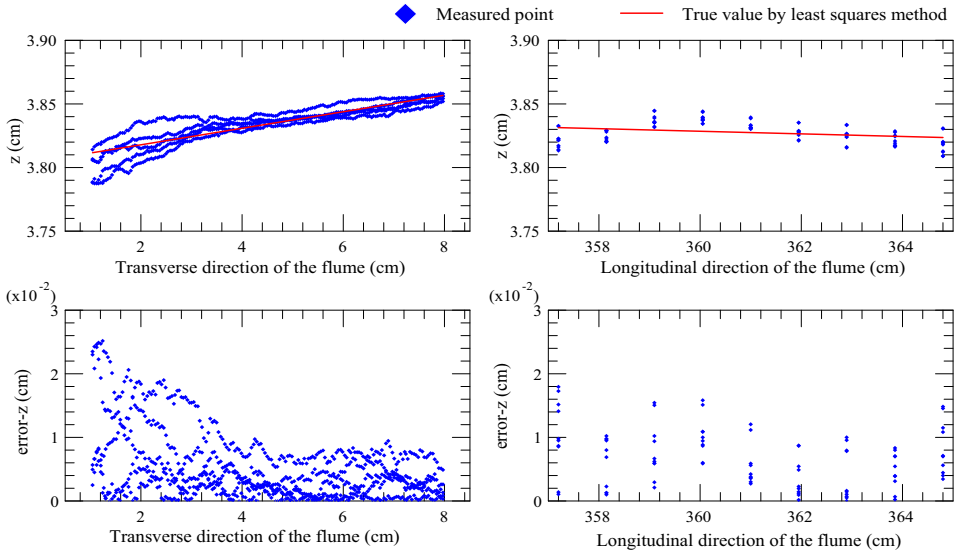

Figure 8. (Left) The upper figure shows the results of transverse measurements on the top surface of a rectangular area under dry conditions. Five measurements at 3 cm intervals in the longitudinal direction were superimposed by blue dots (15 sections in total). The red line is the estimated value obtained by the least-squares method and is regarded as the true value. The lower figure shows the z error between the true and measured values. (Right) As in the left figure, the upper figure shows the measurement results in the longitudinal direction. The results of five measurements at 3 cm in the transverse direction are superimposed.

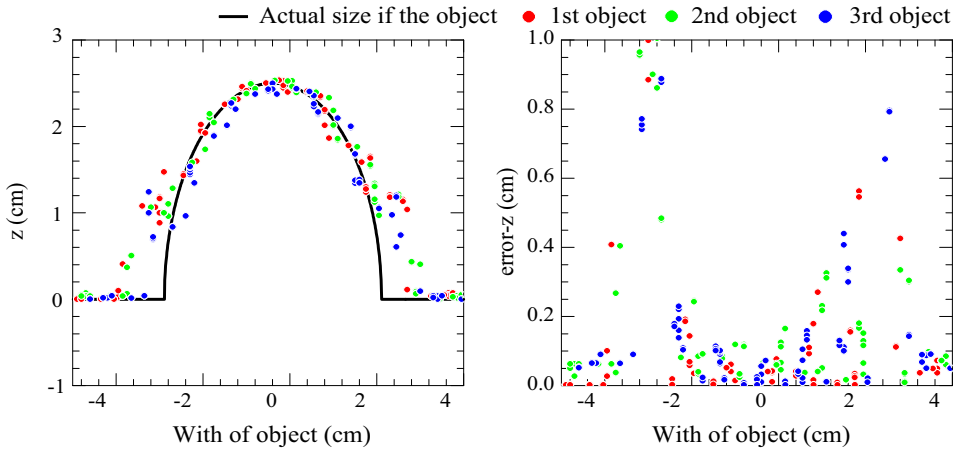

Figure 9. (Left) The results of five measurements in the longitudinal direction for three hemispheres on the right side under dry conditions are superimposed (15 sections in total). The measurement line was chosen to pass through the hemispherical center. The solid black line is the true value, which is a semicircle of radius 2.5 cm. (Right) z error between the true and measured values.

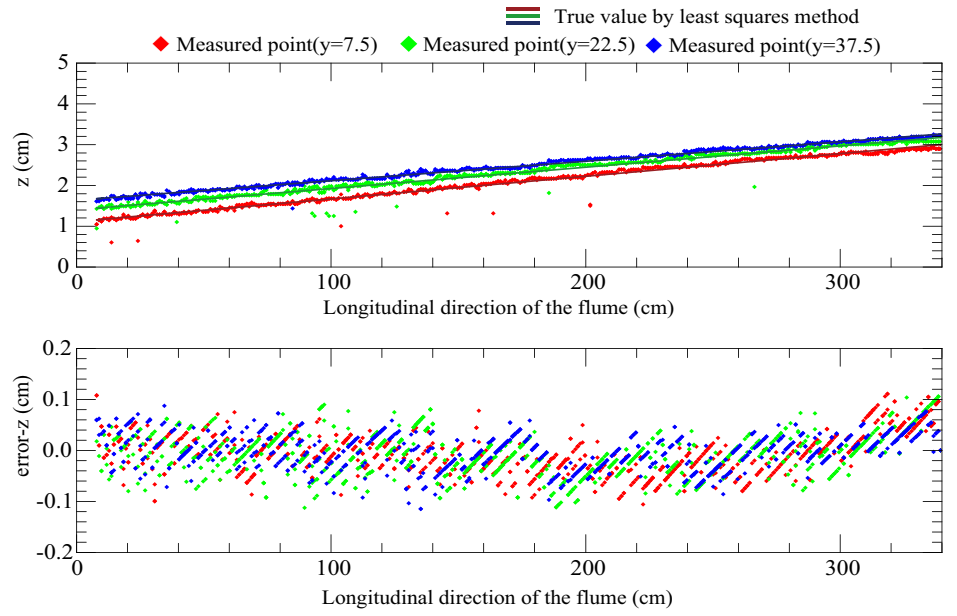

Figure 10. (Upper) The measurement results of the longitudinal section on the still water surface are shown for each measurement line, color-coded according to the distance from the starting point. The water depth increased longitudinally owing to the weir condition. The solid line of each color is the true value obtained using the least-squares method in each lateral direction. (Lower) z error between the true and measured values.

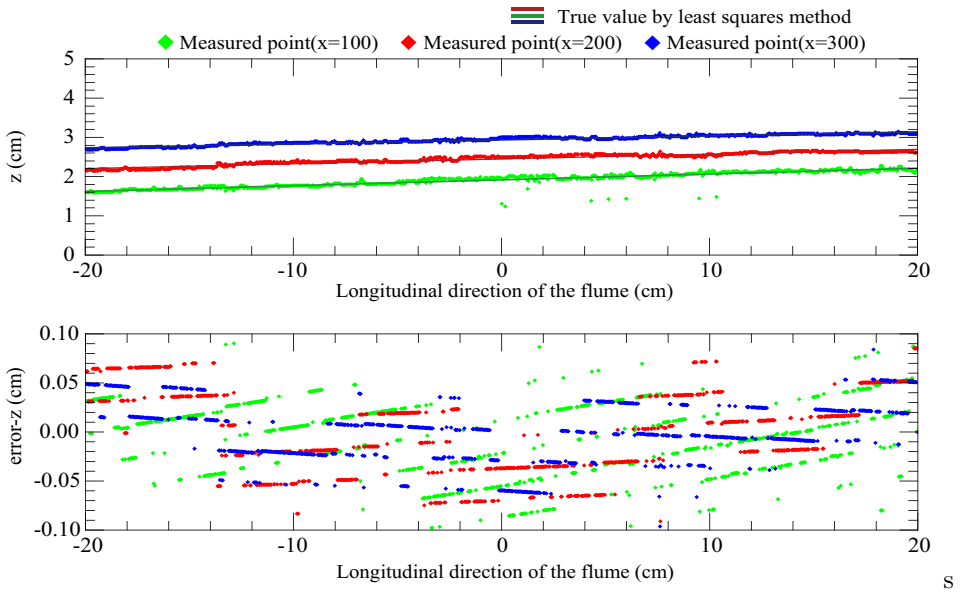

Figure 11. (Upper) The measurement results of the transverse section at the still water surface are shown by color-coding each measurement line according to the distance from the right bank. The solid line of each color is the true value obtained using the least-squares method for each lateral. (Lower) z error between the true and measured values.

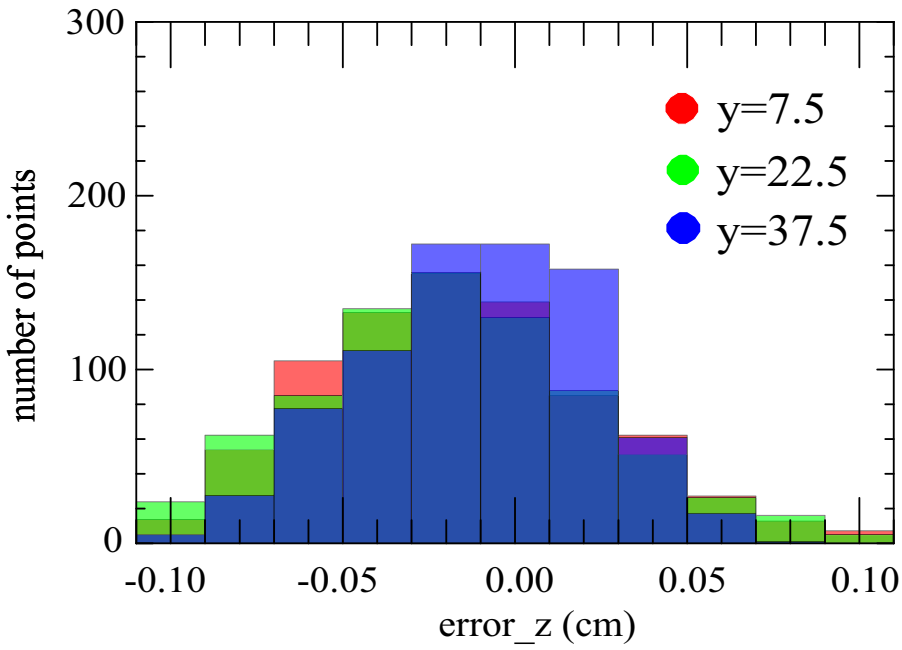

Figure 12. Histogram of the longitudinal z-error in still water surface measurements.

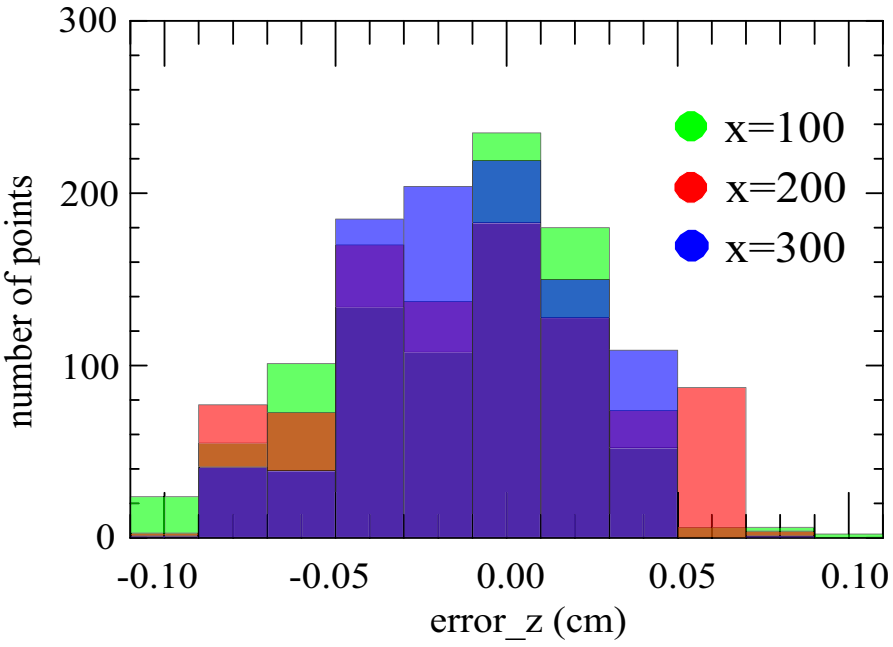

Figure 13. Histogram of the transverse z-error in still water surface measurements.

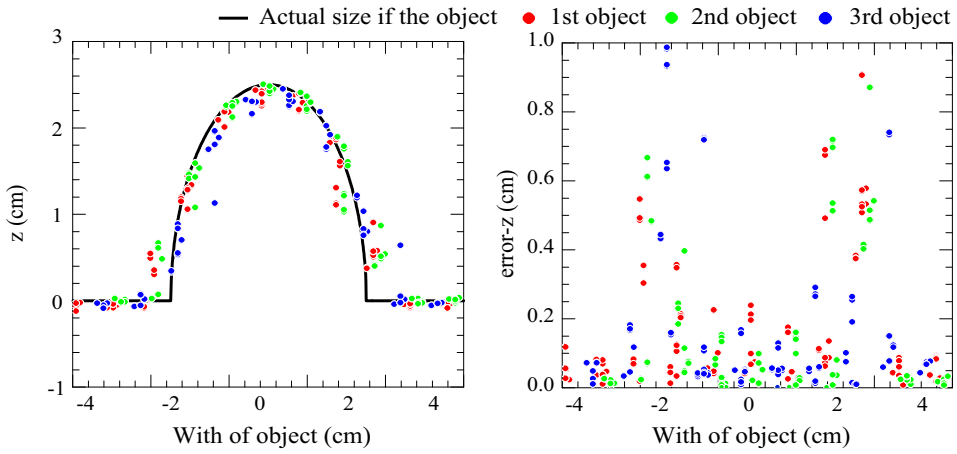

Figure 14. (Left) The results of five measurements in the longitudinal direction for the three hemispheres on the right side under still water conditions are superimposed (15 sections in total). The measurement line was chosen to pass through the hemispherical center. The solid black line is the true value, which is a semicircle of radius 2.5 cm. (Right) z error between the true and measured values.

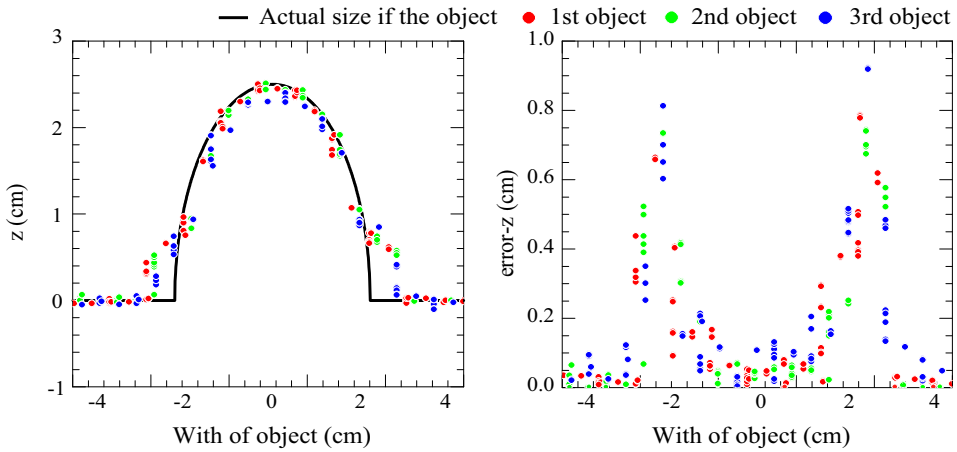

Figure 15. (Left) The results of five measurements in the longitudinal direction for the three hemispheres on the right side under flowing water conditions are superimposed (15 sections in total). The measurement line was chosen to pass through the hemispherical center. The solid black line is the true value, which is a semicircle of radius 2.5 cm. (Right) z error between the true and measured values.

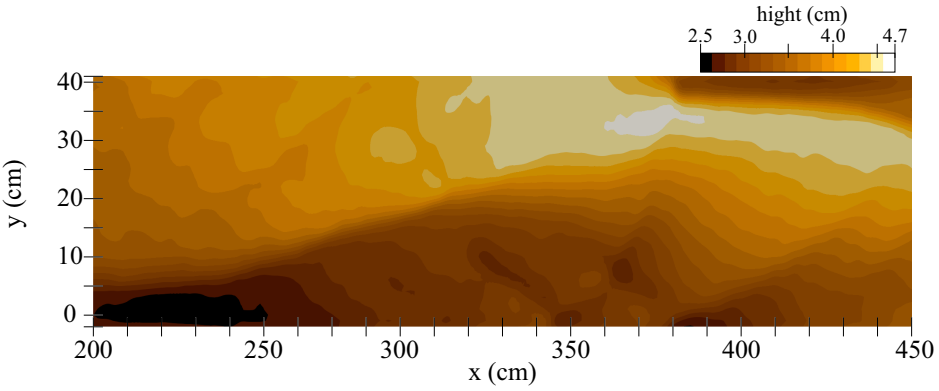

Figure 16. Measurements of the bed of the fixed sandbar cemented after the water flow in Experiment 4. The wave height was just above 2 cm. To avoid the effect of noise near the wall, the area was trimmed by 1 cm on each side.

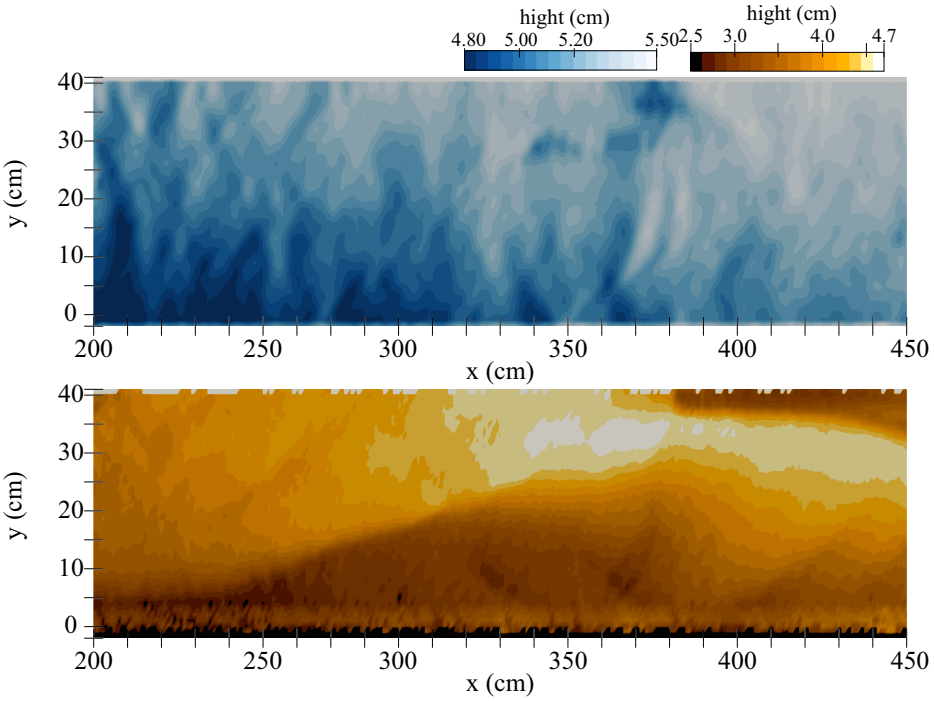

Figure 17. Measurement results of the cemented bed under flowing water conditions. The upper and lower figures show the results of the water surface and bed measurements, respectively.

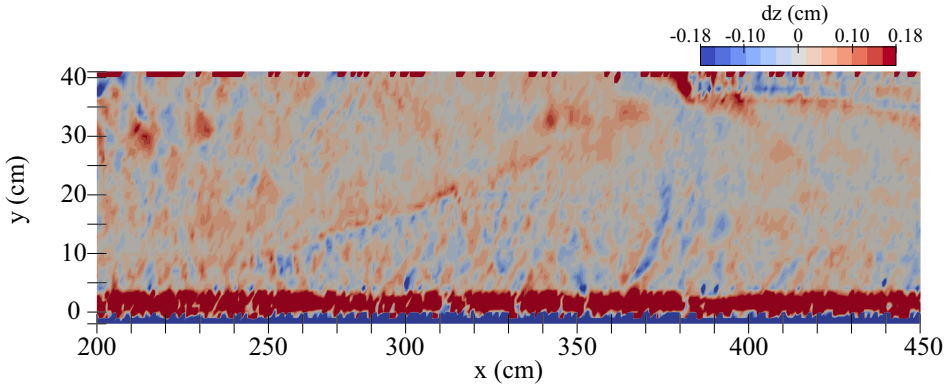

Figure 18. The contour shows the measurement error of the bed surface in the z direction under the flowing water condition, with the true value measured under dry conditions. Excluding the noise on the wall, the maximum error was 2 mm.

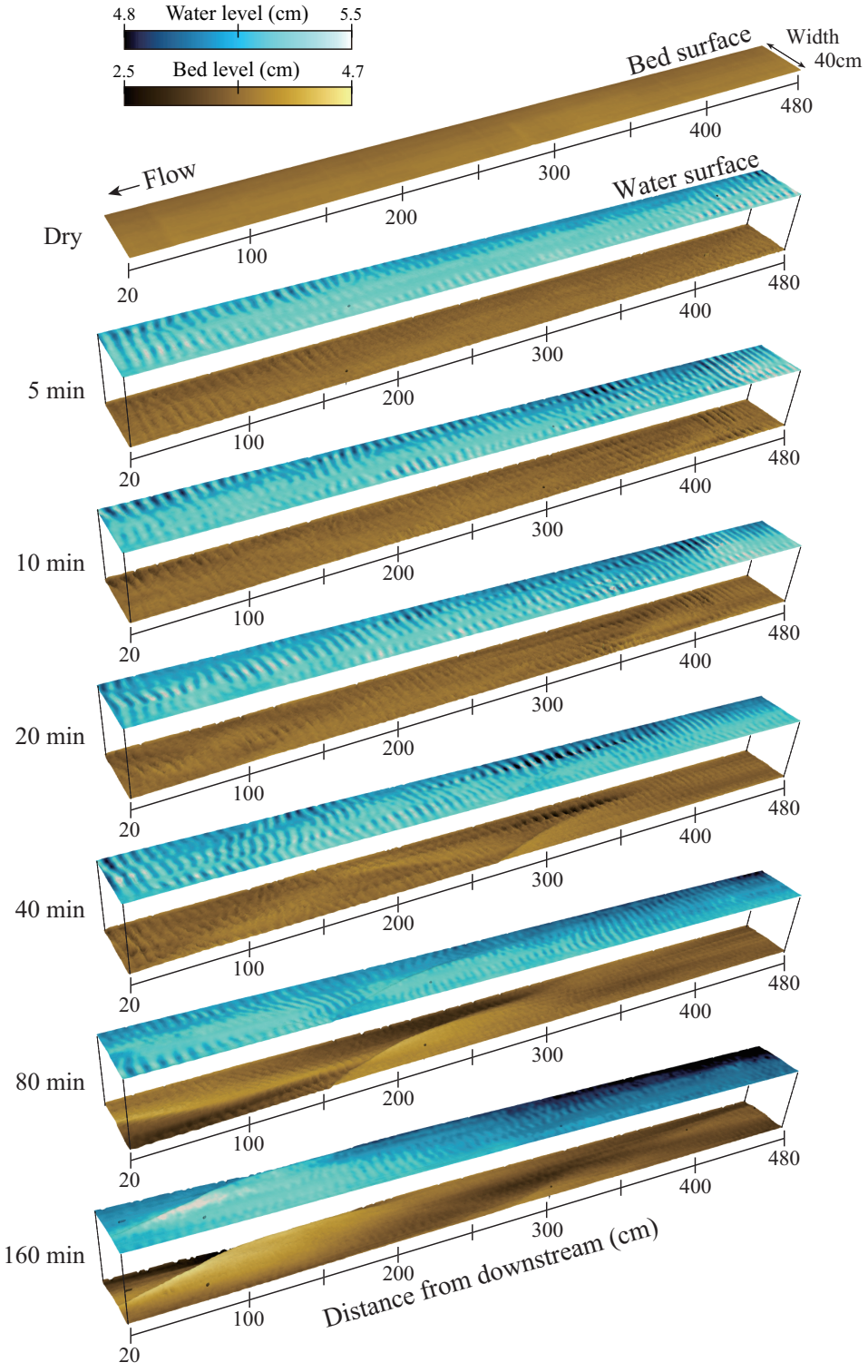

Figure 19. Measurements of the water surface and bed during the formation and development of riverbed waves from a flat bed. The positions of the water surface and bed were independent of water depth. Note the difference in the coloring range between the water surface and the bed.